Journal of Thermal Analysis and Calorimetry (2021) 143:879–898
https://doi.org/10.1007/s10973-020-09363-x

Experimental investigation of convective heat transfer growth on ZnO@TiO_2/DW binary composites/hybrid nanofluids in a circular heat exchanger

Waqar Ahmed[1,2] · S. N. Kazi[2] · Z. Z. Chowdhury[3] · M. R. B. Johan[3] · Naveed Akram[2] · M. A. Mujtaba[2] · M. Gul[2] · C. S. Oon[2]

Received: 1 November 2019 / Accepted: 19 January 2020 / Published online: 5 February 2020

Abstract
The thermophysical properties of freely suspended ZnO and TiO_2 nanoparticles in a base fluid (DW) with different mass% concentrations of ZnO@TiO_2/DW binary composite nanofluids (0.1, 0.075, 0.05 and 0.025 mass%) are deliberated. ZnO have been synthesized by using a facile single-pot sonochemical method and mixed with TiO_2 under high probe sonication to prepare binary composite nanofluid. The experiment of effective thermal conductivity was executed in the temperature range of 20–45 °C. The positive improvement in thermal conductivity value for ZnO@TiO_2/DW binary composite nanofluids was recorded for 0.1 mass%, and the highest improvement was measured up to 36%, greater than the base fluids (DW). The convective heat transfer properties of the ZnO@TiO_2/DW binary composite nanofluids with different concentrations and base fluid (DW) were also examined by using complete experimental test rig with a circular heat exchanger based on a constant heat flux boundary conditions. All the concentrations were examined to check the local and average improvement in heat transfer with Reynolds range from 5849 to 24,544. The increase in nanoparticles mass% in base fluid causes to raise the heat transfer coefficient (h) which is due to the composite nanoparticles. Finally, the maximum 600–1950 W m^{-2} K^{-1} enhancement was found in convective heat transfer with an increase in 0.1 mass% of composite nanoparticles, which is 69% greater than base fluid, while all other concentrations also shows positive enhancement as compared to base fluid (600–1870, 600–1700 and 600–1500) W m^{-2} K^{-1} correspondingly.

✉ Waqar Ahmed
waqarum.ah@gmail.com

✉ S. N. Kazi
salimnewaz@um.edu.my

[1] Institute of Advanced Studies, University of Malaya, 50603 Kuala Lumpur, Malaysia

[2] Department of Mechanical Engineering, Faculty of Engineering, University of Malaya, 50603 Kuala Lumpur, Malaysia

[3] Nanotechnology and Catalysis Research Center (NANOCAT), University of Malaya, Kuala Lumpur, Malaysia

Graphic abstract

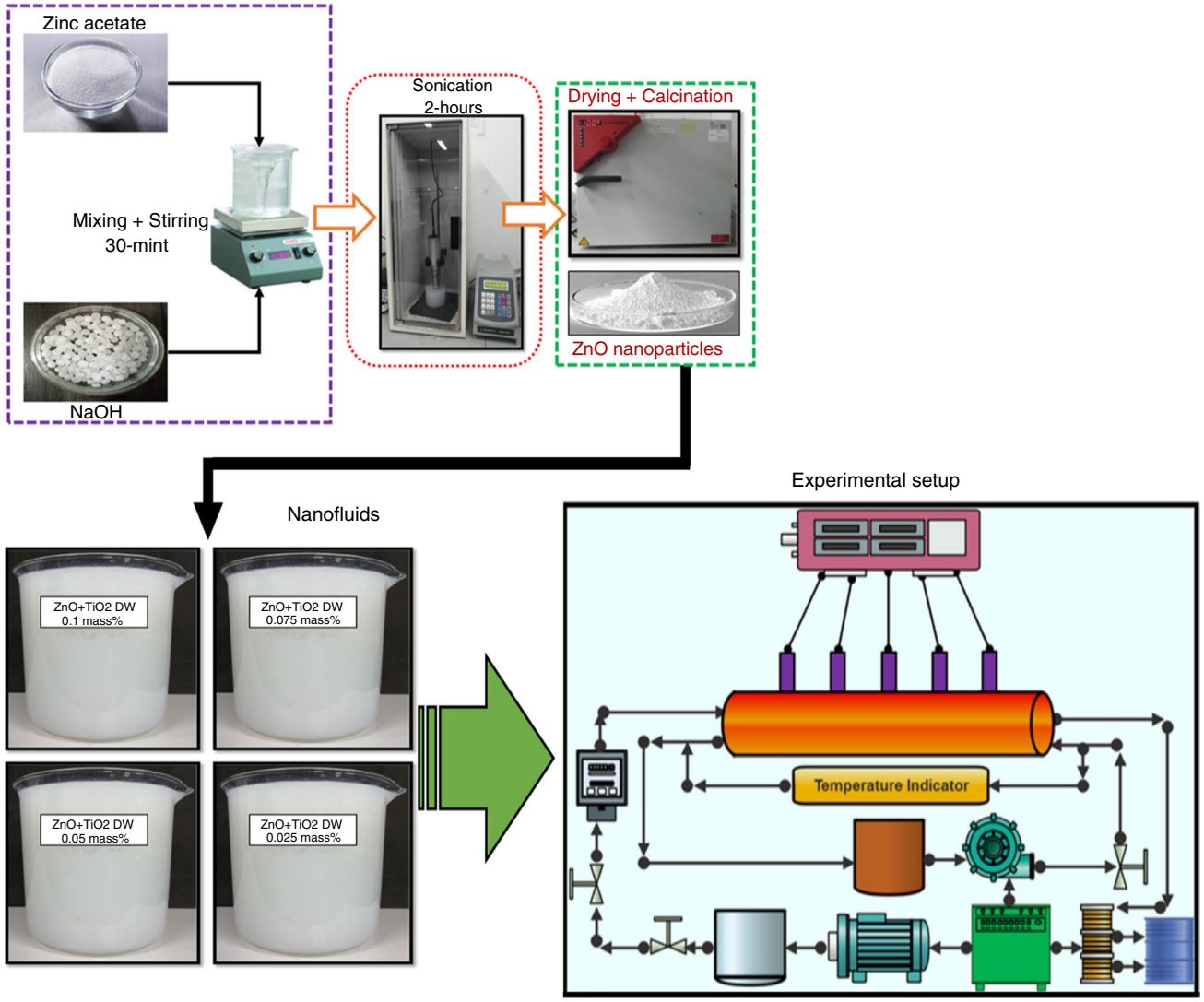

Keywords Nanoparticles · Heat transfer · ZnO@TiO_2/DW binary composites · Nanofluids · Thermal conductivity

List of symbols

Nu	Nusselt numbers
D_h	Pipe diameter
C_{Pnf}	Heat capacity for nanofluid
P_P	Pumping power
Q	Heat flux
f_f	Friction factor
mass%	Particle mass concentration
k	Thermal conductivity (W m^{-1} K^{-1})
I	Inlet condition
PN	Prandtl numbers, $Pr = c_p \cdot \eta / k$
S_{gen}	Entropy ratio
B	Bulk value
c_p	Specific heat (J kg^{-1} K^{-1})
Re	Reynolds numbers, $Re = \rho \cdot v \cdot D / \eta$
FESEM	Field emission scanning electron microscopy
R	Ration of nanoparticles
DW	Distilled water
A	Area of pipe
L	Total length of the test pipe
T_{out}	Outlet temperature
T_{in}	Inlet temperature
T_s	Pipe surface temperature
T_b	Fluid bulk temperature
V	Velocity (m s^{-1})
TC	Thermocouple

Greek symbols

μ	Dynamical viscosity (MPa s)
ρ	Fluid density in (kg m^{-3})
ω	Mass concentration (%)
η	Efficiency

Subscripts

nf	Nanofluid
bf	Value of base fluid
Np	Nanoparticle
Cnf	Composite nanofluid
hnf	Hybrid nanofluids

Introduction

There has been significant interest in improving the different fluids with enhanced thermophysical properties for improvement in the heat transportation of various heat exchangers [1–3]. The recent researches on nanofluids describe that the addition of different highly thermal conductive nanoparticles in the base fluid like DW, EG, PEG, palm oil, diathermic oil, paraffin oil, glycerin, transformer oil, etc. improves the effective thermal conductivity, hence improving the heat transfer values of base fluid [4–6]. Normally, the heat transfer rate of any base fluid is increased by increasing the mass% concentrations; this is because the increased Brownian motion in the base fluid causes the speedy heat transportation from the heat exchanger walls to nanofluid [7, 8]. To improve the thermal energy and heat transfer performances, different studies with different materials and approaches were conducted by many investigators [9]. Consequences presenting in the literature are about closed-loop cooling, and heating offers a considerable role in frequent industrial areas like chemical or petrochemical industries, power plants, automobiles, nuclear, food, microelectronics, solar thermal energy, industrial cooling, electronic cooling, geothermal extraction, magnetic sticking, etc. [10]. To improve the heat transportation, different studies with different metal oxides, ceramics, carbon-based nanoparticles, etc. were considered by a series of researchers [11]. Later, there are massive numbers of opportunities in the present and upcoming time toward expanding the convective heat transfer and energy efficiency of the different thermal systems [12, 13].

The nanomaterial world offers exciting opportunities and challenges for physicists, chemists, biologists and nanomaterial scientists [14]. Nanofluids typically contains the different metals, metal oxides, ceramics and carbon structured nanoparticles, and the most popular solid nanoparticles are Al_2O_3, CuO, TiO_2 and SiO_2 [3]. Furthermore, the thermophysical and chemical properties of nanomaterials can be significantly changed and modified during their synthesis or functionalization which may affect their properties due to their shape and size [15]. Different metallic, bio-waste, metal oxides, ceramics and carbon-based materials have been used to prepare different kinds of nanofluid by using one-step or two-step methods. Such kinds of nanofluids may consist of Al/Al_2O_3, Cu/cupric oxides, ZnO and TiO_2 [16]. In the present time, to improve the heat transfer significant researches have been conducted on metal oxides, composite/hybrids of metal oxides, carbon and carbon-based nanofluids [17], single-wall carbon nanotubes (SWCNTs) [18], multi-walled carbon nanotubes (MWCNTs) [19–21], gold and diamond nanoparticles [22], graphene or graphene oxides [23] and also activated carbon. Activated carbon is usually primed from different organic materials like coconut shells [24], sawdust of coconut trees [25], agro wastes and biomaterials, palm shells, seed coat, rubber tree, cotton stalks, tea leaves, pistachio nutshells, palm shells, biomass waste including corn cobs and different dead leaves that contain high level of carbons [26–29]. The agronomic surplus is a choice of attention due to its little cost and its feature of a source of renewable energy [30].

Since few decades, different nanofluids having good suspension and dispersion with solid nanoparticles have attracted interest due to some experimental reflections of their improved thermal conductivity properties beyond the calculations of the effective test medium theory and their credible applications in the energy-saving field [31–34]. Further, the convective heat transfer models traits the thermal conductivity improvement which effected by Brownian motion, in some other cases it shows less Brownian effects on thermal conductivity. Numerous clustering models have also been suggested, counting clustering with micro-heat convection or clustering with heat conduction [35–37]. Thermal conductivity for suspended alumina nanoparticles was examined using the transient hot-wire technique presented by Nagashima and Nagasaka. The outcomes obtained from experiments describe that effective thermal conductivity will increase with an increase in mass% of alumina oxide nanoparticles [38, 39]. The experiments were conducted to measure the thermal conductivities of a nanocomposite system composed of unsaturated polyester resin (UPR) as medium and two dissimilar metal oxide nanoparticles as a filler: Al_2O_3 and CuO are presented here. The used nanoparticles were alpha (Al_2O_3 30–40 nm and CuO 30–50 nm). Different samples were made up by using simple physical blending and magnetic stirring. Thermal conductivities for each sample were inspected using a device that obeys with (ASTM C518-04 and E1530-06). All the measurements were repeated at different temperatures (0, 25 and 50) °C with different concnentrations of the Al_2O_3 and CuO nanofluids; and the results are compared with different models to ensure the positive enhancement in thermal conductivity after using metal oxide-based nanofluids [40, 41]. Efforts are needed to enhance the thermal conductivity and heat transfer

properties of nanofluids; in this context, metal oxide-based composite nanofluids were examined here. Some of the consequences arise from that literature about composite nanofluids are listed in Table 1.

The key objective of this research is to study the effective transportation of convective heat transfer by using metal oxide-based ZnO@TiO_2/DW binary composite nanofluids by changing mass% concentrations (0.1, 0.075, 0.05 and 0.025). Distilled water with ZnO@TiO_2 composite can transport the benefit of the blend of binary metal oxides where ZnO@TiO_2 can stimulate the overall thermal conductivity and heat transfer properties of the suspended nanoparticles with slight sedimentation. Previously, a few investigations were practiced about thermophysical properties of binary composite nanofluids by using different metal oxides. The efforts were made here to improve the heat transfer value of a circular heat exchanger by using sonochemically synthesized ZnO (17 nm) particles and commercially purchased TiO_2 (21 nm) physically blended in water for heat transportation studies. In the present experimentation at specific range of Reynolds numbers (Re), the local Nusselt values (Nu), average Nusselt values, local heat transfer and average convective heat transfer at different points crosswise, the circular heat exchange in the turbulent and transitional areas of flow was evaluated for the ZnO@TiO_2/DW binary composite nanofluids at different (0.1, 0.075, 0.05 and 0.025) mass% concentrations (Fig. 1).

Table 1 Characteristics of different composite nanofluids from the previous literature

Composite nanofluid	Nanoparticle size and shape	Methodology	Different parameters/variables	Thermal conductivity measurement	Efficiency in terms of thermal conductivity	Reference
AIN (aluminum nitride)–EG	30 nm	Two-step; sonication time 150 mint	(1–4%) con, flow rate 0.4–4 LPM, 25–50 °C, laminar, R/N 500–1750			[42]
Al_2O_3–MWCNTs (18–15)–thermal oil	Al_2O_3 20 nm The 20–30 nm diameter of MWCNTs	Two-step 7-day stability	Conc: 0.125–1.5% 25–50 °C, laminar and turbulent	5% accuracy KD2 Pro 0.02–2 W m^{-1} K^{-1} Needle Dm 1.3 mm	1.5% for Al_2O_3 And 45% for 50 °C	[43]
Al_2O_3–Cu (50/50) EG	Cu 70 nm Al_2O_3 5 nm	Two-step + 7-h sonication	Cu 2%–Al_2O_3 0.125% 25–50 °C	ND: 1.3 mm NL: 6 cm KD2 Pro, 5%	2% Al_2O_3–Cu 28%-50 °C	[44]
Ag/MWCNTs/water	Ag 30 nm MWCNTs 10 nm	Two-step 3-h sonication	Ag–MWCNTs: 0.1% 20–50 °C	Accuracy 5% KD2 Pro	20.4%-40 °C 0.1% Ag–MWCNTs	[45]
Al_2O_3/MWCNTs/water	Al_2O_3: 30–50 nm MWCNTs 20 nm	Two-step 1-h sonication 5-day sedimentation UV, for stability	Ag 1,2 and 4% Al_2O_3–MWCNTs 1–6%, 15–40 °C Al_2O_3–MWCNTs = 90:10, 97.5:2.5	Hot-wire method Lambda system	Nonground MWCNTS 12–4% hybrid 90:10	[46]
Al_2O_3–CuO/EG water 25:75	Al_2O_3 40 nm CuO 29 nm	Two-step 16-h sonication	Cu + Zn, 2.0–0.5% 23–25 °C	Hot-wire method Lambda system	CuO–Al_2O_3 90–95%	[47]
Al_2O_3–Cu/water	Al_2O_3–Cu 17 nm	Two-step Stability checked by zeta potential and pH	Al_2O_3, 0.1–2% 20–60 °C Surfactant–SLS	Accuracy 5% Range 0.2–2 W m^{-1} K^{-1} KD2 Pro	12.11–2% Cu–Al_2O_3	[48]
Ag–MgO/water	Ag 25 nm MgO 40 nm	Two-step 3-h sonication	Temp 25 °C, pH 5.57 Surfactant–CTAB Conc: Ag–MgO (0–2%)	ND 1.27 mm KD2 Pro Accuracy 5% NL 6 cm	Ag 16% Ag–MgO 2%	[49]
Ag–graphene nanoparticles/water	GNP 2 µm	Two-step	Conc: Ag = 0.02% GNP = 0.1% Temp: 20–40 °C RN = 5000–17,500 Flow = Turbulent	ND = 1.3 mm NL = 6 cm KD2 Pro Accuracy = 5%	40 °C for 22.22% and 0.1% Ag–GNP	[50]
Al 5, mass% Zn	Al–Zn 10–30 nm	Two-step	Conc: Zn 5 mass% 0.01–0.1% Temp: 30–70 °C	KD2 Pro	16% for 0.1% Al 5 Zn mass%	[51]

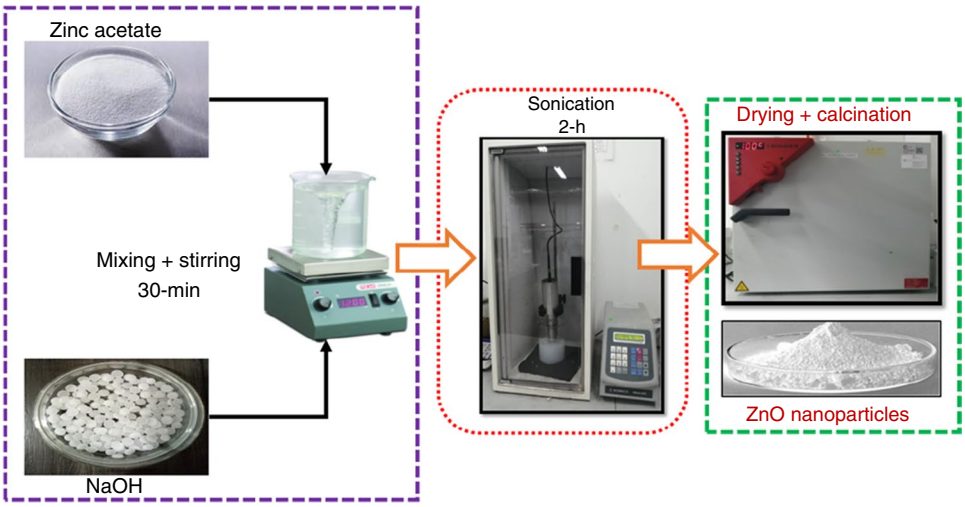

Fig. 1 Synthesis of ZnO by facile single-pot sonochemical technique

Materials and methods

The procedure adopted in this investigation is graphically signified in Fig. 2. Primarily the ZnO nanoparticles were synthesized by using single-pot sonochemical synthesis and confirmed by XRD, FTIR, UV–Vis and FESEM characterizations. The synthesized ZnO nanoparticles were diluted and sonicated in distilled water for a specific time without using any surfactant. Titanium (IV oxide 99.5% trace metals basis) nanoparticles were purchased by chemical provider company Sigma-Aldrich Sdn Bhd, Malaysia. Furthermore, a typical two-step nanofluid preparation method was used to synthesis the ZnO@TiO_2/DW binary composite nanofluids. An investigation on the thermophysical properties of prepared nanofluids was carried out and reported hereafter, confirming the dispersion and stability of nanofluids in the base fluid (DW).

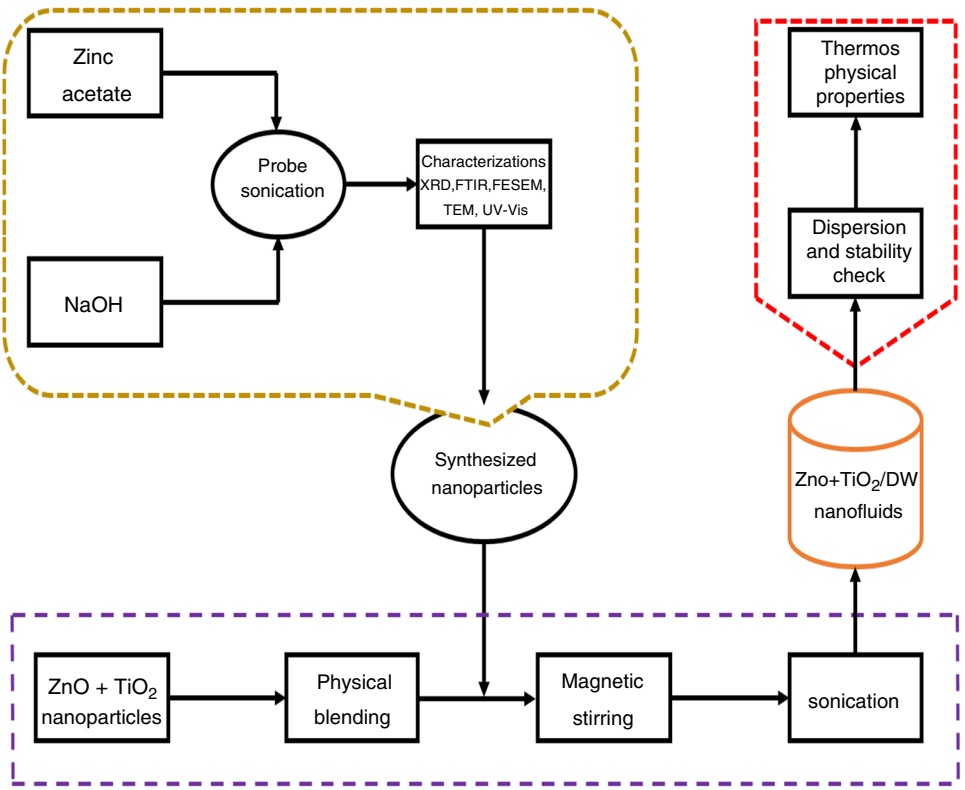

Fig. 2 Procedure for the preparation of ZnO@TiO_2/DW binary composite nanofluids

Synthesis of ZnO by using single-pot sonochemical technique

In the stated experimentation, it is commended a single-pot sonochemical synthesis of ZnO in order to enhance its dispersion and stability by using zinc acetate (precursor) analytical reagent and sodium hydroxide (base) analytical reagent. In this synthesis, zinc acetate was diluted in a 100 mL mixture of ethylene glycol and distilled water with a 50:50 mL of each according to 2:1 molarity and stirred for half an hour. Sodium hydroxide (NaOH) was also diluted in 100 mL mixture of ethylene glycol and distilled water solution with 50:50 mL each under constant stirring for a half an hour. Finally, sodium hydroxide (NaOH) solution has been dropped into zinc acetate solution dropwise under constant probe sonication. The sonicator of SONICS (CV 334 Vibro cell) company has been used for sonication. The sonicator power was adjusted 750 watts; the pulse amplitude was fixed on 80% with 3/2 s on/off time, the net distributed probe energy 36,000 J and the input voltage 220. After dropping the base solution into zinc acetate solution, the mixture has been left for 2-h continuous sonication. During the addition of sodium hydroxide NaOH into zinc acetate mixture, white precipitates appear into the beaker. With time passage, it changed into thicker white precipitates. The precipitates appear during the reaction and were washed by water several times by using a centrifuge machine with 6000 rpm, and lastly, once it was washed with ethanol. Further for drying the sample, it has been kept in a heat oven overnight at 100 °C. For crystallization and specific shape, the dried sample has been kept for calcination at 200 °C in a high-temperature furnace for 3 h uninterruptedly.

Preparation of ZnO@TiO_2/DW binary composite nanofluids

The offered study concerns the use of physical blended ZnO and TiO_2 in base fluid (DW) nanoparticles by using probe sonication technique for heat transfer measurements. ZnO nanoparticles were synthesized by using a single-pot sonochemical procedure, while TiO_2 was procured by chemical provider company Sigma-Aldrich Sdn Bhd, Malaysia. The ZnO and TiO_2 nanoparticles were blended physically in base fluid (DW) with the initial mass% concentration of 0.1, 0.075, 0.050 and 0.025, respectively. Later the both ZnO and TiO_2 nanoparticles were mixed with 50:50 each in base fluid (DW) and sonicated for 3 h without using any surfactant. The experimentations were led at four different nanoparticle blend ratios (0.1, 0.075, 0.050 and 0.025) mass%. Moreover, the presented procedure shows the well-dispersed and well-suspended ZnO and TiO_2 nanoparticles in base fluid (DW) with 50:50 each by mass ratios. Later on, the dilution procedure is commenced with the assistance of Eqs. (1) and (2). The two-step flow of composite nanofluids preparation is given in Fig. 2, where it can be seen in the first step ZnO nanoparticles have been synthesized; then, TiO_2 nanoparticles were mixed together in base fluid (Tables 2, 3; Fig. 3).

$$\emptyset = \frac{\omega \rho b_{\mathrm{f}}}{\left(1 - \frac{\omega}{100}\right)\rho p + \frac{\omega}{100} \times \rho b_{\mathrm{f}}} \tag{1}$$

$$\Delta V = (V2 - V1) = V1\left(\frac{\emptyset 1}{\emptyset 2} - 1\right). \tag{2}$$

Stability and dispersion of ZnO@TiO_2/DW binary composite nanofluids

The ZnO_2@TiO_2/DW binary composite nanofluids were physically blended by high probe sonication procedure to increase the dispersion and suspension of the nanoparticles in base fluid and to decrease the agglomeration [52]. The four samples of 50 mL each with different mass% (0.1, 0.075, 0.05 and 0.025) was prepared and sonicated for a specific time by using probe sonication to achieve good dispersion and stability. Then these samples were physically tested for sedimentation and dispersion of nanoparticles in base fluid after preparation until 14 days. The nanoparticle dispersion and stability in base fluid depend upon their particle size and sonication time, where the smaller size particles offer longer suspension [53]. The sedimentation reflection for ZnO@TiO_2/DW binary composite nanofluids is shown in Fig. 4. Subsequently, after 14 days of sample preparation, the ZnO@TiO_2/DW binary composite nanofluids with different (0.1, 0.075, 0.05 and 0.025) mass% concentrations are experiential to be still stable as displayed in Fig. 4. The estimation of the given nanofluids' suspension and stability was also examined through ultraviolet–visible (UV–Vis) spectral analysis. The absorbance and the light scattering are restrained by associating the ZnO@TiO_2/DW-based nanofluid light intensity with base fluid [54]. The physical observations elaborate the good dispersion and stability of both nanoparticles in the base fluid until 14 days after its preparation time without using any surfactant.

Table 2 Characteristics of ZnO, TiO_2 and water (50:50) mixture

Characteristics	ZnO	TiO_2	Base fluid/DW
Color	White	White	Colorless
Size of particles	17 nm	21 nm	–
Purity	97.9	99.9	–
Mass concentrations	50	50	–

Table 3 Mass concentrations of ZnO and TiO_2 with base fluid (DW)

S. no	Mass% concentration	Base fluid in litters	ZnO nanoparticles in grams	TiO_2 nanoparticles in grams	Total nanoparticles in grams
1	0.1	7	3.5	3.5	7
2	0.075	7	2.265	2.265	5.25
3	0.05	7	1.75	1.75	3.5
4	0.025	7	0.87	0.87	1.75

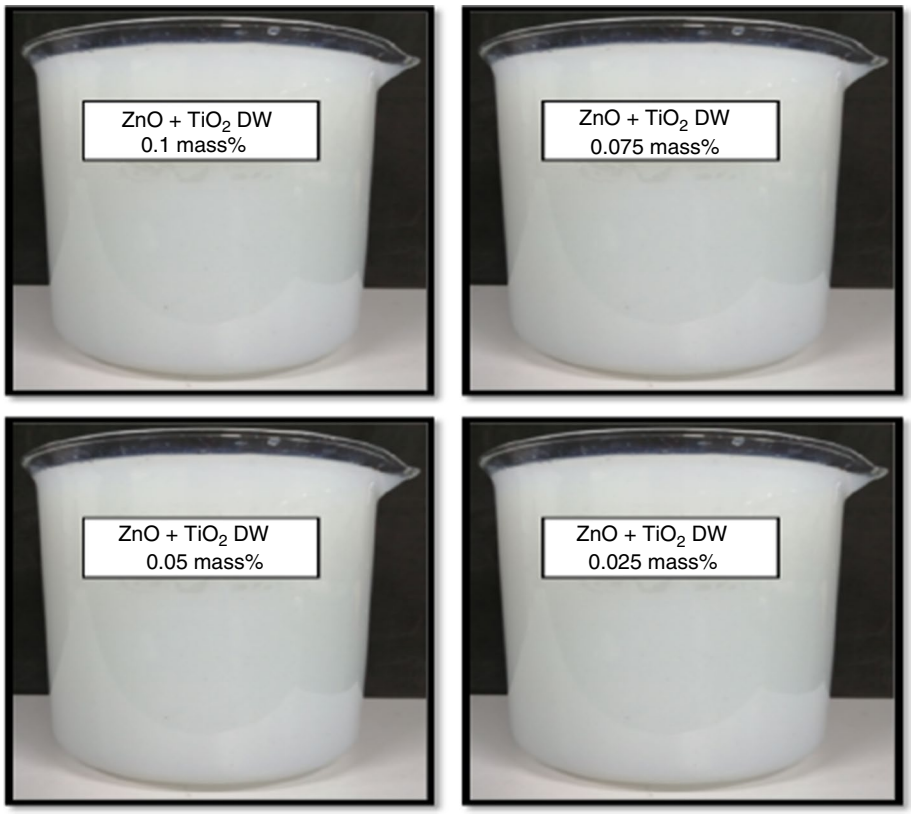

Fig. 3 ZnO@TiO_2/DW binary composite nanofluids with different mass% concentrations

Thermal conductivity of ZnO@TiO_2/DW binary composite nanofluids

Figure 5 shows an experimental setup of the KD2 Pro thermal analyzer (Decagon Devices) company to compute the thermal conductivity values by implementing the ASTM-D5334 and IEEE 442-(1981) standard for ZnO@TiO_2/DW-based nanofluids. The shown instrument follows the transient line convective heat source to measure the nanofluid's thermal properties. The thermal conductivity experiment was commenced for a specific series of temperatures starting from 20 to 45 °C. To keep the constant temperature during the experiment, a cooling system has been used. The KD2 Pro sensor needle sensor was validated by defining the thermal conductivity of the normal confirmation liquid of glycerin given by the same company. The calculated value was 0.285 W m^{-1} K^{-1} with a precision of ±0.34%. The experiment was repeated frequently, and the average calculation among five repetitions of readings was deliberated. The presented thermal conductivity calculations are considered for different time intervals to maintain the temperature each before the new calculation for each sample at a series of temperatures for ZnO@TiO_2/DW binary composite nanofluid mass% concentrations. This is most significant to diminish the errors during an experiment by free heat convection owing to the variations in temperature along with the KD2 Pro needle sensor, which is directly connected to the fluid sample. The four different mass% concentrations (0.1, 0.075, 0.05 and 0.025) of ZnO@TiO_2/DW-based nanofluids were tested here.

Test section geometry

A circular test pipe of stainless steel with 1400 mm all-out length and 0.01 m internal diameter from two sides is

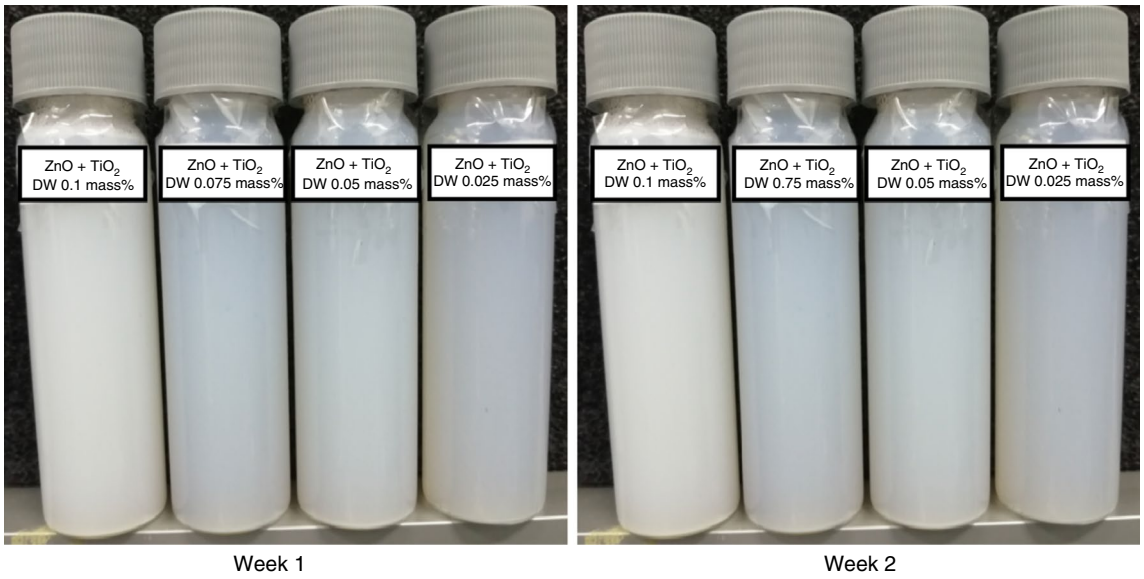

Fig. 4 Stability and sedimentation of $ZnO@TiO_2$ nanoparticles in distilled water

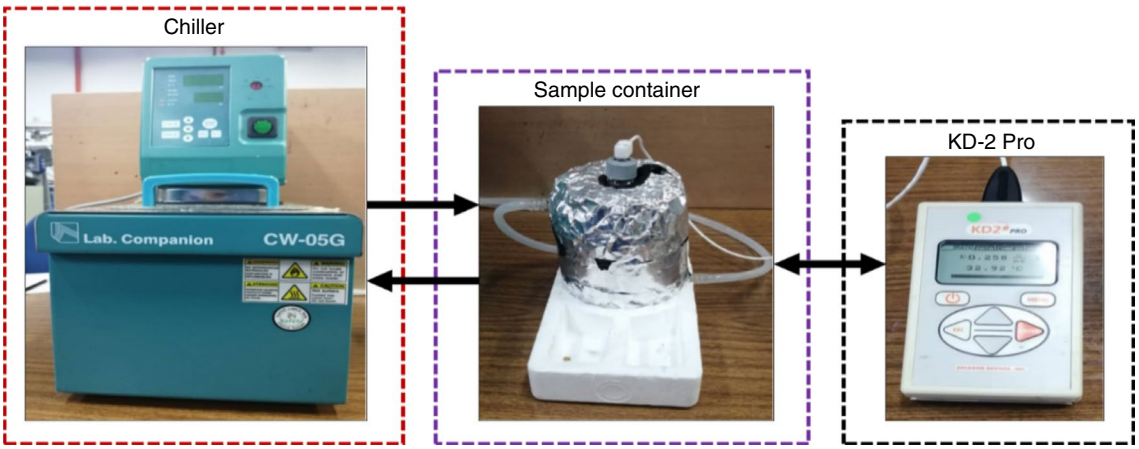

Fig. 5 Experimental setup for thermal conductivity measurement by using KD2 Pro analyzer

the key part of the experimental setup and used as a heat exchanger. The heated position of the circular test section was wrapped by electrical heat tape up to 1200 mm length with maximum 900 W capacity which is fully controlled by voltage transformer. A thick layer of wool insulation has been twisted alongside the circular test section and covered by the aluminum foil to stop the heat releasing by pipe surfaces. Five highly sensitive K-type thermocouples are placed at various points at the surface of a circular test pipe separated from others with equivalent separation of 0.2 m of each. Close to channel, inlet and outlet, thermocouples are additionally joined with this test section to quantify the temperature distinction (Fig. 6).

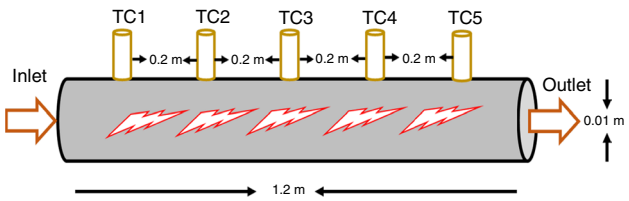

Fig. 6 Circular heat exchanger with thermocouples arrangements

Experimental

The experimental studies of this research work were conducted in a test rig shown in Fig. 7 which comprises of a major fluid flow loop with bypass, fluid pump, fluid tank,

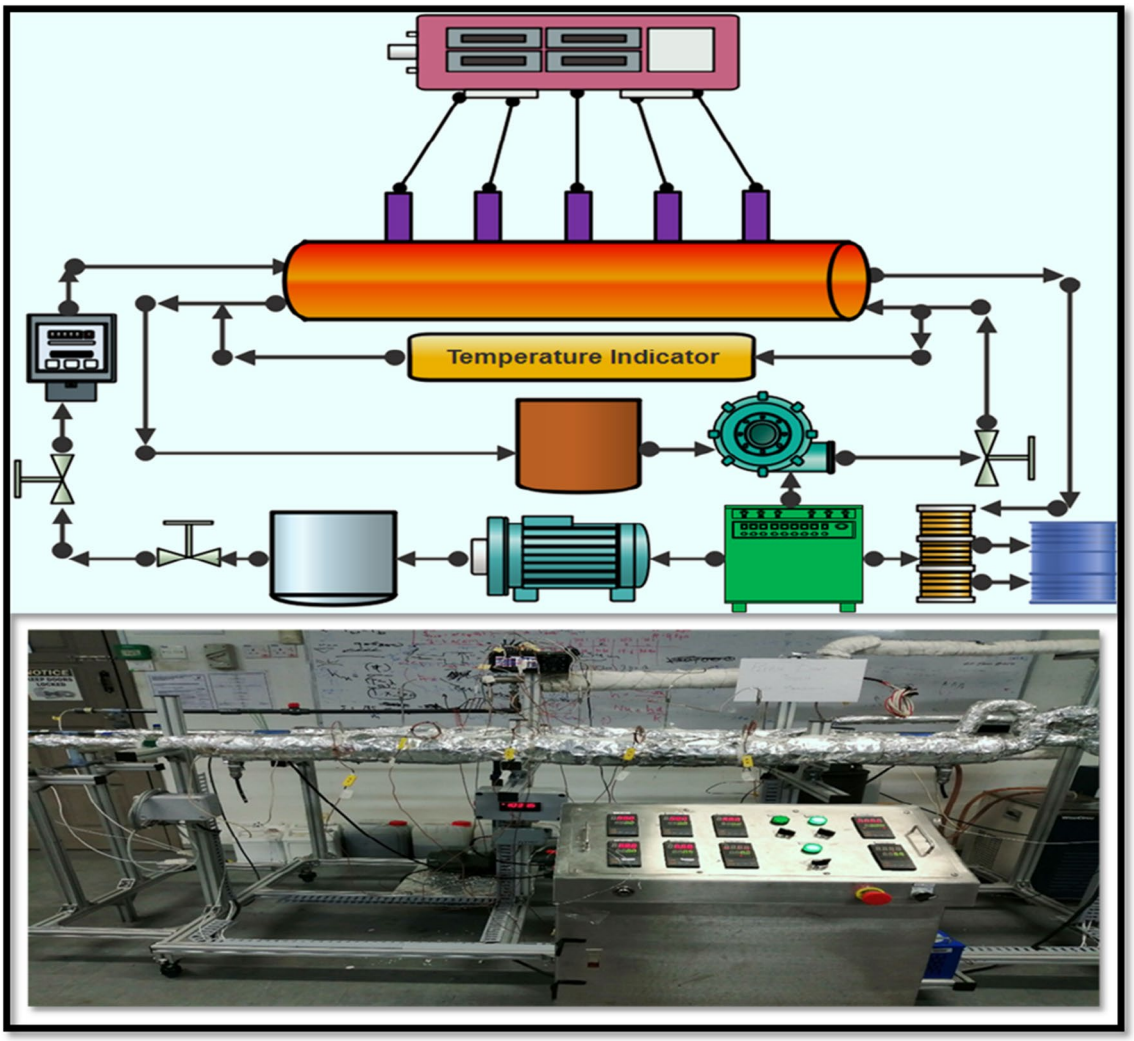

Fig. 7 Pictorial and schematic diagram of heat transfer experimental test rig with different parts

digital flow meter, pressure drop meter, inlet and outlet valves, pressure gage, coolant/chiller, K-type sensitive thermocouples, main power supply, digital data logger (Graphtec GL220) and the full test section as shown in the schematic diagram. The experimentation flow loops started with 10 L capacity fluid tank where the nanofluid were stirring uniformly and chiller is used to maintain temperature constant. The nanofluids flowing through the flow loop were pumped by an Araki/EX-70R fluid pump with maximum capacity 88L/mint and about zero discharge heads of total 6.8 m. Then the pump flow values can be changed by controlling frequency according to requirement from main panel control. The total pressure drop during the nanofluid flow has been measured by using PX154/025DI OMEGA pressure transducer with maximum accuracy ± 0.075%. Prior to running the nanofluid on the experimental setup, the appropriate positioning of the test section is the most important task to quantify the circular test pipe surface temperature and to clarify the presence of convection of nanofluids in the circular heat exchanger. In this way, we connected the thermocouples at various points in the track of the circular heat exchanger and surface temperature by means of logical wholes by applying the Wilson plot appeared [55]. Further, the thermophysical properties of ZnO@TiO_2/DW composite nanofluids were examined by scheming the Nusselt numbers (Nu), pressure drop (Pa/m), friction factor loss (f_f) and local and average convective heat transfer (h) values. By applying the Newton cooling law for inlet and outlet temperatures and its difference, nanofluid temperatures and medium surface temperature, we can compute the convective heat transfer coefficient.

Uncertainties in heat transfer experimental setup

The presented investigations are on ZnO@TiO_2/DW binary composite nanofluids for convective heat transfer capacities,

Table 4 Uncertainties counted during the testing of the ZnO@TiO_2/DW-based nanofluids

S. no	Parameters	Symbols	Uncertainty/%
1	NF inlet temperature	T_{in}	±0.14
2	NF outlet temperature	T_{out}	±0.14
3	Ambient temperature	T_e	±0.14
4	NF mass flow rate	v	±1.9
5	NF differential pressure	h_h	±2.2
6	NF thermal conductivity	k_{nf}	±2.4
7	NF specific heat measurement	C_{pnf}	±2.9
8	Voltage	V	±0.15
9	Current	I	±0.15
10	Heat flux	Q	±0.15
11	Reynolds numbers	Re	±0.2
12	Convective heat transfer	h	±2.9
13	Nusselt numbers	Nu	±2.9
14	Pumping power	P_P	±2.3

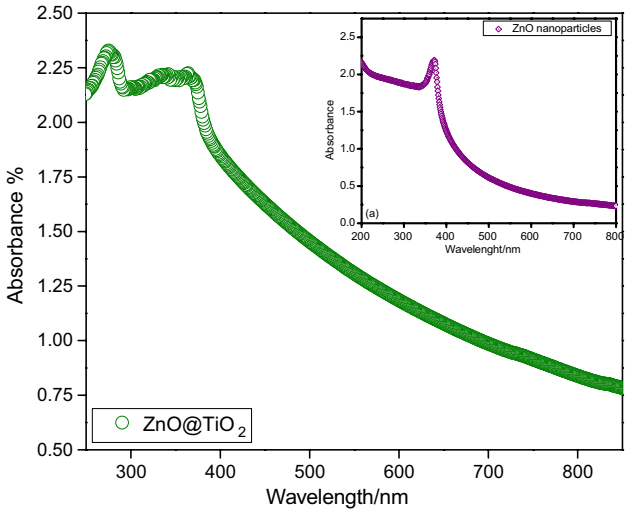

Fig. 8 UV–Vis spectra for ZnO and ZnO@TiO_2/DW binary composite nanofluids

the total velocity, variation in temperatures, volume flow rates, overall pressure drop, Reynolds (Re) and Nusselt (Nu) values, which were inspected with appropriate equipment's arrangements. Throughout the experimental capacities of these above-mentioned parameters, the uncertainties occurred are presented in Table 4. Sighted the linked errors in the distinct factors signified by (x_n) error approximations of reliant parameters was whole by using the below-given equation [56]. The different uncertainties were counted for proposed investigational results and are given in Table 4. Numerous time repetition approach expresses that each parameter of given investigational consequences is within the uncertainty limits.

$$W = \frac{[(x1)2 + (x2)2 + \cdots + (xn)2]}{2}. \quad (3)$$

Results and discussion

UV–Vis spectral analysis

UV–Vis spectral analysis is a common procedure to confirm the optical behavior of the sonochemically synthesized zinc oxide. The UV–Vis (1800 spectrometer) Shimadzu Corp 0.8579 has been used for the analysis of ZnO nanoparticles. The UV–visible spectrometry for the synthesized ZnO-based nanofluids of 0.025 mass% concentration is shown in Fig. 8. The highest absorbance peak at 370 nm specifies the successive synthesis of ZnO, which is owing to the blue lateral shift to the ZnO in bulk amount. The absorption level augmented its energy band gap from 3.37 to 3.6 eV [57].

Similar inspections of different nanofluid dispersion and stability by using UV–Vis spectral analysis were earlier suggested and deliberated by others [58, 59]. The ZnO@TiO_2/DW binary composite nanofluid absorbance values for probe sonication time and nanoparticle sedimentation time were observed frequently up to specific time and detailed wavelength from 200 to 850 nm. The four samples with different mass% concentrations have been sonicated for 3 h each, and this sonication time was noticed to be the maximum stability with an absorbance value of more than 80% for up to two weeks of sedimentation period. Lee et al. and Habibzadeh et al. [59, 60] also suggested comparable results for optimal stability. In the meantime, the stability and dispersion for different samples with time were noticed to be less than 50% of the absorbance ratio after 7 days of physical reflection. By this condition, each sample declines with sedimentation time.

FESEM analysis of ZnO@TiO_2/DW binary composite nanofluids

The morphology, nanoparticle size and chemical composition of ZnO nanoparticles were considered by energy-dispersive X-ray spectrometry (EDX-Zeiss Supra 35/VP) and field emission scanning electron microscopy (FESEM). Field emission scanning electron microscopy (FESEM) has been used to perceive the uniform dispersion stability and shape/morphology of ZnO and TiO_2 in the distilled water [61]. The FESEM images for ZnO, TiO_2 and ZnO@TiO_2 composite nanofluids at 0.1 mass% concentration are shown in Fig. 9. The given FESEM images of composite nanofluids highlight the shape, size and equal dispersion of ZnO and TiO_2 nanoparticles.

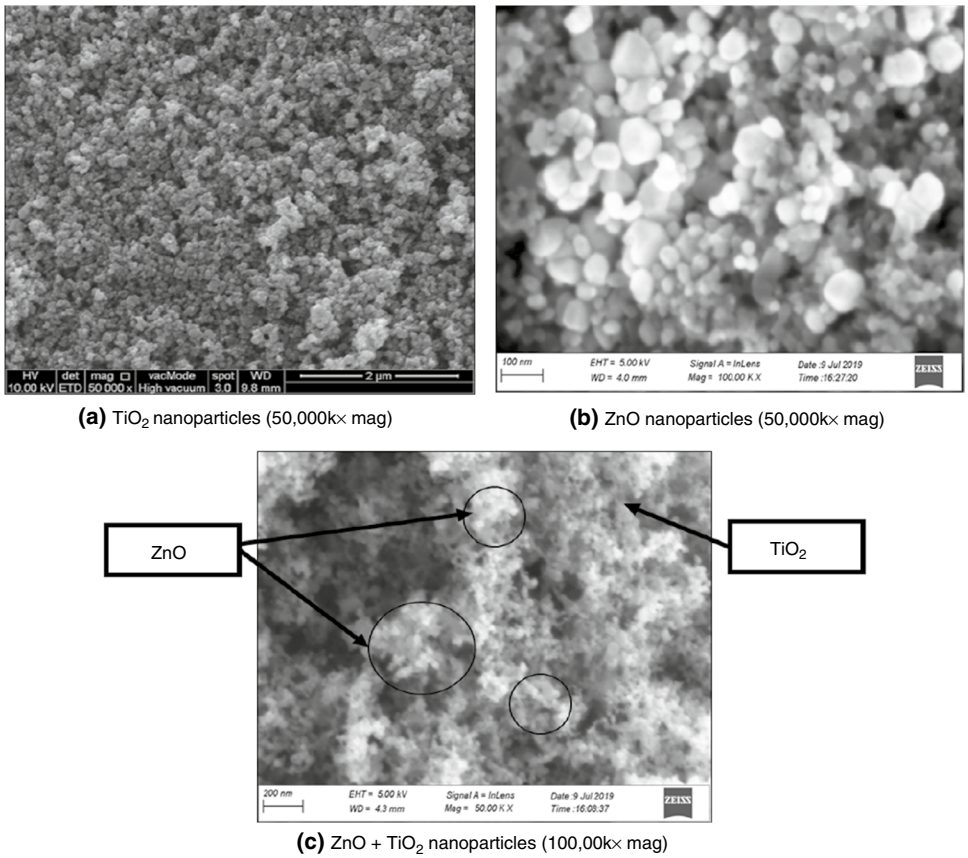

Fig. 9 FESEM images for ZnO, TiO_2 and ZnO@TiO_2 binary composite nanofluids

(a) TiO_2 nanoparticles (50,000k× mag) **(b)** ZnO nanoparticles (50,000k× mag)

(c) ZnO + TiO_2 nanoparticles (100,00k× mag)

Meanwhile, the size of ZnO is less than as compared to the TiO_2, and the space between the nanoparticles of TiO_2 is filled with ZnO nanoparticles. The equal nanoparticle distribution of ZnO@TiO_2 is given in Fig. 9. In general, the contribution of both nanoparticles powerfully depends on the composite's ratios, which signify the mass% of each nanoparticle in the base fluid (DW). This condition led to decrease space among the larger nanoparticles, which gives the benefits to the thermal properties like specific heat and overall thermal conductivity. Furthermore, the thermophysical properties as if density and viscosity are also anticipated changing by this condition. In order to assess the distinct characteristic for both nanoparticle distributions, the current effort explores the effects of nanoparticle composite concentrations on effective thermal conductivity of ZnO@TiO_2/DW-based nanofluids.

Thermophysical and hydrodynamic properties of ZnO@TiO_2/DW-based binary composite nanofluids

Figure 10 displays the linear growth in thermal conductivity values for ZnO@TiO_2/DW binary composite nanofluids with a range of temperatures from 20 to 45 °C for (0.1, 0.075, 0.05 and 0.025) mass% concentrations. The thermal conductivity values of ZnO@TiO_2/DW composite nanofluids for all given mass% concentrations increased with increase in temperature, which are compariitvley greater than base fluid. Additionally, it has been noticed the highest thermal conductivity value was recorded with an equal ratio of ZnO@TiO_2 for 0.1 mass% concentration of a given fluid. Meanwhile, the 0.025 mass% delivered the lowermost thermal conductivity value among all composite concentrations for all temperatures ranges. The outcomes confirmed the increased percentage of ZnO and TiO_2 contribute equally to the greater thermal conductivity value of the ZnO@TiO_2/DW binary composite nanofluids as presented in Fig. 10. In the current exploration, the relation of composite mass% ratios to the thermal conductivity value improvement might be owing to the dissimilar size of the two different nanoparticles and the

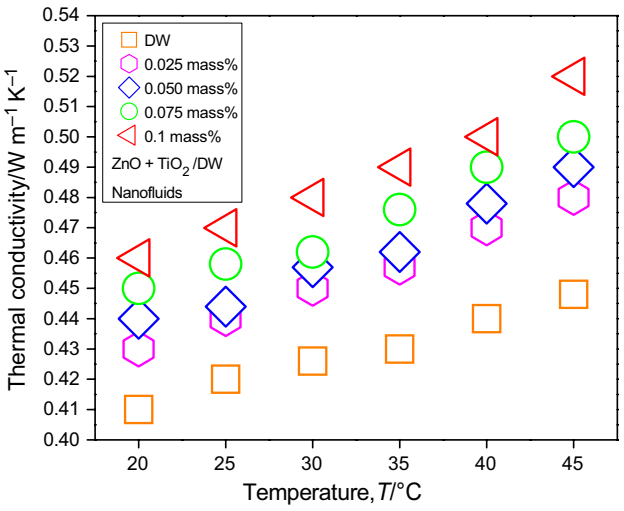

Fig. 10 Growth in thermal conductivity with temperature for (DW, 0.025, 0.05, 0.075 and 0.1 mass%) ZnO@TiO_2/DW binary composite nanofluids

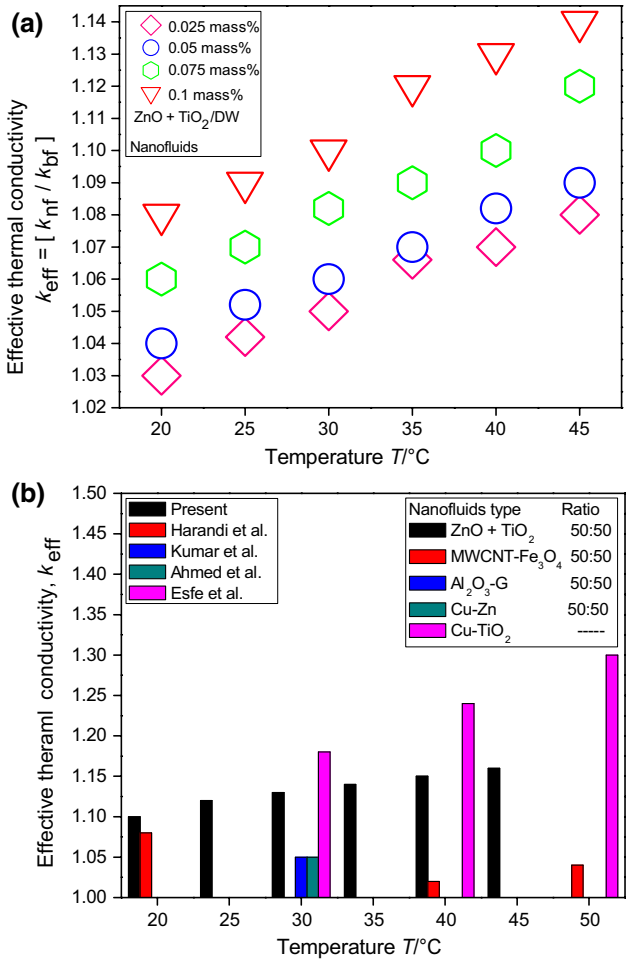

Fig. 11 **a** Variations in effective thermal conductivity with temperature for (DW, 0.025, 0.05, 0.075 and 0.1 mass%) ZnO@TiO_2/DW binary composite nanofluids, **b** comparison of thermal conductivity with the literature

quantity of the lesser nanoparticles existing in the composite. The average diameter of ZnO nanoparticles is 17 nm, which is lesser than the TiO_2 nanoparticles of 21 nm. The ZnO nanoparticles support in thermal conduction by filling the space among the large TiO_2 nanoparticles, as shown in the FESEM images given in Fig. 9. The characteristic procedure of the two different nanoparticles in the composite dilution will increase the contact area for thermal conduction among the different molecules and hence persuade a greater amount of thermal heat transfer during the collision process by the Brownian motions [62].

The effective thermal conductivity values of ZnO@TiO_2/DW binary composite nanofluids and its associated improvements against different values of temperatures are given in Fig. 11a, respectively. The outcome exposes the effective thermal conductivity value and grows with an increase in mass% of ZnO nanoparticles in the ZnO@TiO_2/DW in the binary composite nanofluids, excluding for the 0.025 mass% ratio with the lowermost effective thermal conductivity value of given nanofluids. The effect of different temperature values on the overall effective thermal conductivity value is also significant. Furthermore, the supreme augmentation has recorded at the maximum value of the temperature of 45 °C with an improvement of 36% for 0.1 mass% of ZnO@TiO_2/DW binary composite nanofluids. This could be owing to interaction among all nanoparticles which is triggered by kinetic energy at high temperature and the effects of Brownian motion [63]. Figure 11b describes the comparison between present outcomes and literature data of effective thermal conductivity from Hardani et al. [63], Kumar et al. [64], Ahmed et al. [65] and Esfe et al. [66].

In order to describe the pressure drop changes across the circular test section, we present the total pressure drop for binary composite of ZnO@TiO_2/DW with all mass% concentrations and base fluid (DW) as a function of specific Reynolds numbers. Figure 12a shows that there is a slight increase in pressure drop for the all mass% concentrations of binary composite nanofluids compared to base fluid. The maximum pressure drop was noticed across the section for 0.1 mass% concentration, and we belive this increase is due to little increment in dynamic viscosity of the binary composite nanofluid, which requires little increase in composite nanofluid velocity against the Reynolds. Here, we concluded the velocity of composite nanofluid plays an important role in increasing the friction factor and pressure drop as well.

Our target is to avoid a radical increase in dynamic viscosity of the ZnO@TiO_2/DW binary composite nanofluids, where greater amount of viscosity can increase the pumping power. Therefore, we calculate the dynamic viscosity of

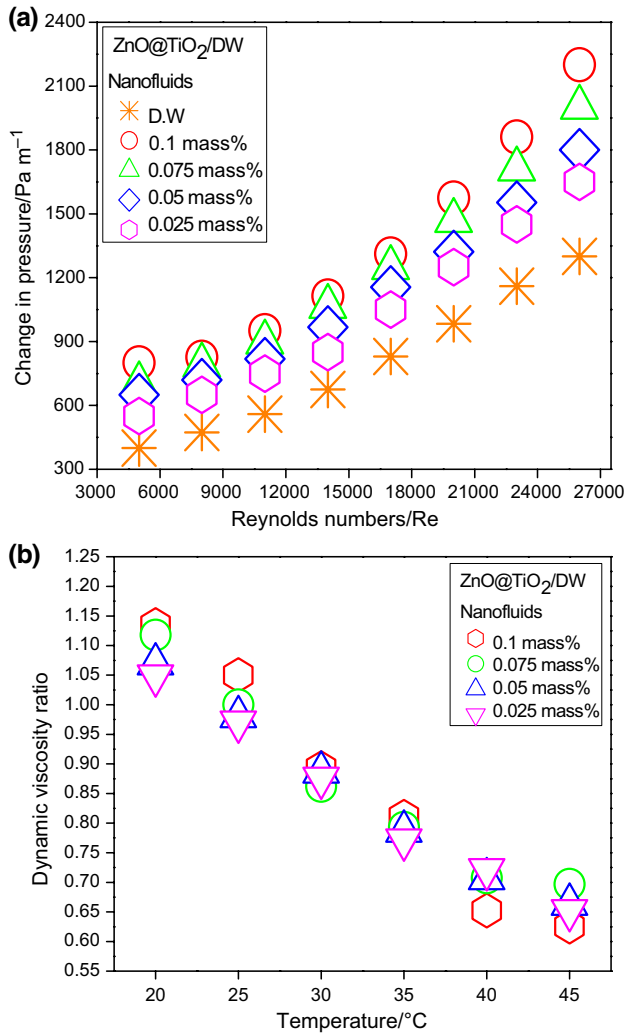

Fig. 12 **a** Pressure drop profile for DW and different mass% concentrations of ZnO@TiO_2/DW binary composite nanofluids, **b** dynamic viscosity of ZnO@TiO_2/DW binary composite nanofluids

the ZnO@TiO_2/DW binary composite nanofluids with 0.1, 0.075, 0.05 and 0.025 mass% concentrations and temperature range from 20 to 45 °C in Fig. 12b. It can be seen when we rise the mass% of both nanoparticles in base fluid, there is a slight increase in the viscosity of binary composite nanofluids related to distilled water. In fact, these are expected changes because we only used very low concentration of both ZnO and TiO_2 nanoparticles in our nanofluid samples. It can be observed the dynamic viscosity of the binary composite nanofluids is dependent upon temperature changes, once the temperature increases the dynamic viscosity of both nanofluids and water decrease, which is due to weak intermolecular interaction. We concluded we can prevent our samples from dynamic viscosity loss by maintaining and keeping synthesis parameters under control. Further it is necessary to realize the higher mass% cause to increase the dynamic viscosity, while lower mass% prevents the sample from viscosity decrement.

Growth in average heat transfer and average Nusselt numbers of ZnO@TiO_2/DW binary composite nanofluids

Investigation were directed to calculate the average heat transfer coefficient and average Nusselt increase in ZnO@TiO_2/DW binary composite nanofluids running in a closed circular heat exchanger. Necessary calibrations of complete experimental setup are needed before running the sample to grasp the internal surface temperatures of the circular section, in order to analyze the supreme presence of convective heat conduction in the circular tube walls as well as heat convection of the binary composite nanofluid running inside the circular heat exchanger. According to the Wilson plot the resistance among the different points of the test section in direction of surface temperature and heat transfer amount of the circular heat exchanger were calculated by using different mathematical calculations. The stated research considered the thermophysical properties of the binary composite nanofluids and base fluid (DW) by using these factors: thermal conductivity, viscosity, density, specific heat, heat transfer coefficient (h), pumping power, Nusselt (Nu) numbers and pressure drop. On the basis of Newton cooling law for the bulk amount of inlet, outlet and surface temperatures, the heat transfer coefficient has been calculated. The stated study reveals the accumulation of different types of nanoparticles in any base fluids displays improved convective heat transportation and Nusselt (Nu) numbers. In the current investigation, the effect of ZnO@TiO_2/DW binary composite nanofluids with mass% concentrations of 0.1, 0.075, 0.05 and 0.025 on the average heat transfer and local heat transfer (h) coefficients at the constant heat flux and Reynolds from 5849 to 24,544 was inspected. To continue experimentation, average convective heat transfer was measured for ZnO@TiO_2/DW binary composite nanofluids at individually of the stated mass% concentrations for comparison with base fluid. In Fig. 13a, the mounting trends evidently portray that the heat transfer coefficient (h) is growing as the ZnO@TiO_2/DW binary composite nanofluids mass% is increasing. For the base fluid (DW), it can be seen that the convective heat transfer was small due to the nonexistence of ZnO and TiO_2; by adding nanoparticles, the average convective heat transfer coefficient was improved. Figure 13a shows at 0.1 mass% concentration, the convective heat transfer coefficient was greater as compared to base fluid (DW) data. For the base fluid (DW), average heat transfer was recorded from 600 to 800 (W m^{-2} K^{-1}), while in the case of 0.1 mass% ZnO@TiO_2/DW binary

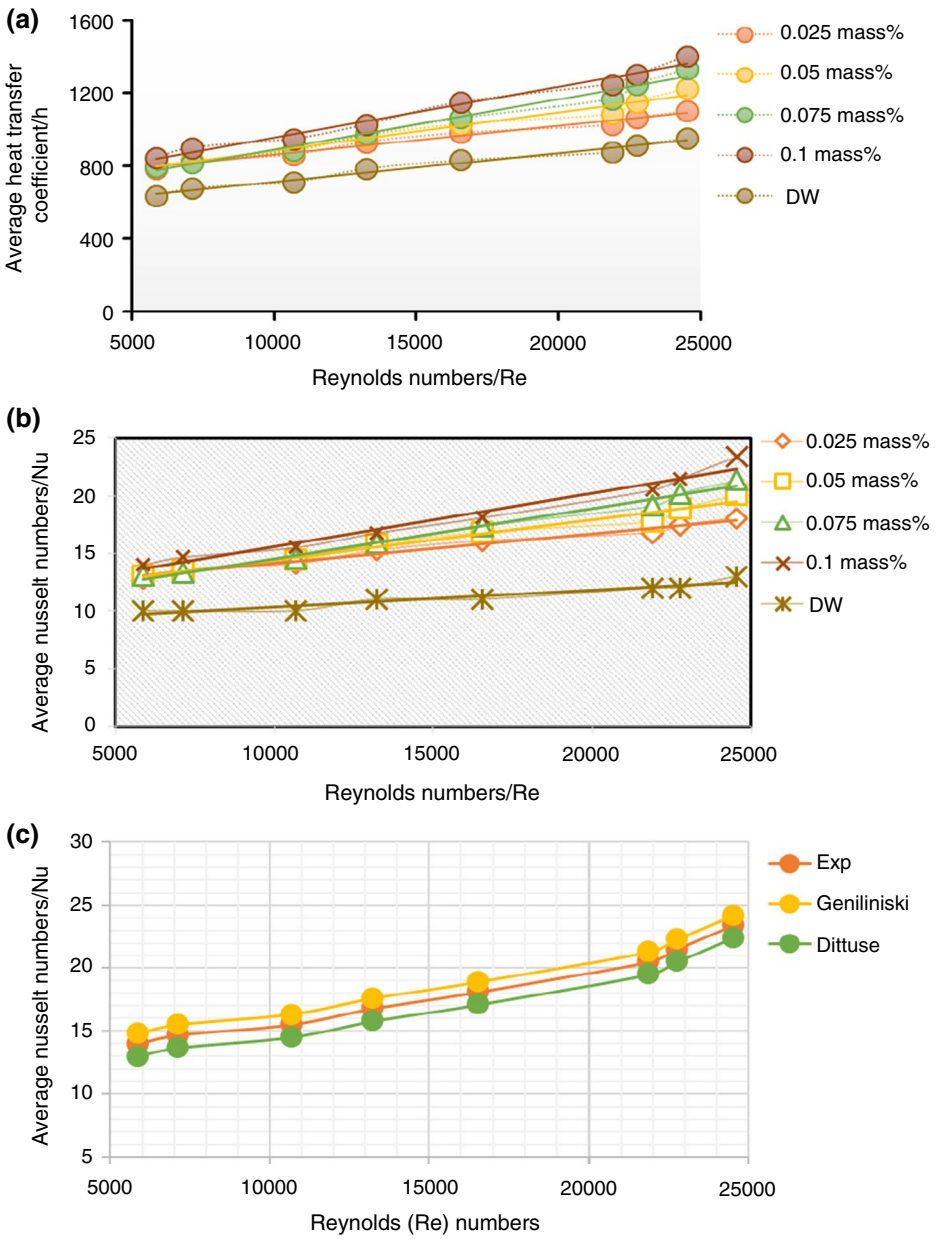

Fig. 13 **a** Average heat transfer measurements, **b** average Nusselt numbers measurements for (DW, 0.025, 0.05, 0.075 and 0.1 mass%) ZnO@TiO_2/DW binary composite nanofluids, **c** comparison of experimental data with model data

composite nanofluid, the highest average heat transfer value was recorded up to 500–1100 W m^{-2} K^{-1}.

Also, experimental data have been used to compute the convective heat transfer and pressure drop characteristics for ZnO@TiO_2/DW binary composite nanofluids. Reynolds (Re) number of base fluid (DW) and ZnO@TiO_2/DW binary composite nanofluids with different (0.1, 0.075, 0.05 and 0.025) mass% concentrations can be measured based on the above-given experimental setup mass velocity and hydraulic diameter of the circular pipe heat exchanger as given below.

$$h = \left(\frac{q''}{Tw - Tb}\right) \tag{4}$$

$$q'' = \left(\frac{Q}{A}\right) \tag{5}$$

$$A = \pi d^2/4 \tag{6}$$

Figure 13a portrays the improvement in average Nusselt (Nu) numbers for the mass% concentrations of ZnO@TiO_2/DW binary composite nanofluids with the increase in the Reynolds (Re) number from 4550 to 20,367. It can be experiential that the average Nusselt (Nu) values for the

base fluid (DW) vary from 9 to 13 with the increase in the Reynolds (Re) numbers. After adding ZnO and TiO_2 in base fluid (DW), the optimistic improvement in the Nusselt (Nu) numbers was perceived, which might be credited to the increase in mass% concentrations level. At 0.1 mass% of ZnO@TiO_2/DW binary composite nanofluid, the supreme improvement in Nusselt (Nu) numbers was noted by the change in Reynolds (Re) numbers from 5849 to 24,544. The Nusselt (Nu) numbers were higher than those noted for the base fluid (DW) without any nanoparticle addition. All the outcomes were confirmed by numeric calculations, as given in Eqs. (7), (8), (9), (10) and (11).

$$\mathrm{Nu} = \left(h \times \frac{D}{K}\right) \tag{7}$$

For the calculation of local and average Reynolds numbers, Eq. (6) can be used.

$$\mathrm{Re} = \left(\frac{\rho v D}{\mu}\right) \tag{8}$$

The empirical correlation of Nusselt numbers was suggested by Dittus–Boelter [67], Gniellinski [68] and Petukhov [69], respectively.

$$\mathrm{Nu} = \left(\frac{\left(\frac{f}{8}\right)(\mathrm{Re} - 1000)\,\mathrm{Pr}}{1 + 12.7\left(\frac{f}{8}\right)^{0.5}(\mathrm{Pr} \wedge 2/3 - 1)}\right) \tag{9}$$

here Re = Reynolds number, Pr = Prandtl number and f = friction factor.

$$\mathrm{Nu} = \left(\frac{\left(\frac{f}{8}\right)\mathrm{Re}\,\mathrm{Pr}}{1.07 + 12.7\left(\frac{f}{8}\right)^{0.5}(\mathrm{Pr} \wedge 2/3 - 1)}\right) \tag{10}$$

If $3 \times 10^3 < \mathrm{Re} < 5 \times 10^6$ and $0.5 < \mathrm{Pr} < 2000$, then Eq. (7) can be used.

$$\mathrm{Nu} = \left(0.023\mathrm{Re}^{0.8}\mathrm{Pr}^{0.4}\right) \tag{11}$$

Lastly, the experimental outcomes were matched with Dittus and Gnielinski models, which give promising comparison among all experimental data and different model data. It displays the combination of ZnO@TiO_2/DW binary composite nanofluids shows improved heat transfer value as compared to model data. Figure 13c describes the average Nusselt numbers obtained from experiments, and the relevant model data showed rising trend with rise in Reynolds (Re) numbers. Here, this binary composite nanofluid is considered to be appropriate selection for heat transfer in engineering applications.

Growth in local heat transfer and local Nusselt numbers of ZnO@TiO_2/DW-based nanofluids

Figure 14a–d represents the local conduct of convective heat transfer for all the mass% concentrations of ZnO@TiO_2/DW binary composite nanofluids. For 0.1 mass% concentration ZnO@TiO_2/DW composite nanofluids, the local convective heat transfer (h) coefficients recorded from 600 to 1900 W m^{-2} K^{-1} at the constant Reynolds (Re) numbers from 5849 to 24,544. For 0.075 mass% ZnO@TiO_2/DW binary composite nanofluid concentration, the local convective heat transfer (h) coefficients were noticed from 600 to 1800 W m^{-2} K^{-1} at the Reynolds (Re) numbers from 5849 to 24,544. For 0.05 mass% concentration of ZnO@TiO_2/DW binary composite nanofluid, the convective heat transfer (h) coefficients were recorded from 600 to 1700 W m^{-2} K^{-1} at the Reynolds (Re) numbers from 5849 to 24,544. In Fig. 13d, it can be perceived as the lowest local convective heat transfer (h) coefficients were measured from 500 to 1750 W m^{-2} K^{-1} for the same Reynolds (Re) numbers specified earlier.

Figure 15a–d displays the different variations in local Nusselt (Nu) numbers against the different ranges of Reynolds (Re) and different mass% like 0.1, 0.075, 0.05 and 0.025 of ZnO@TiO_2/DW binary composite nanofluids. During the experiment, the outcomes professed the local Nusselt (Nu) numbers and were increasing with the rise in Reynolds (Re) in a circular pipe heat exchanger. Figure 14a–d shows that at all of the detailed concentrations of ZnO@TiO_2/DW binary composite nanofluids, the local Nusselt (Nu) values are growing with the variation of Reynolds (Re) numbers. In the case of 0.1 mass% ZnO@TiO_2/DW composite nanofluid, the local Nusselt (Nu) numbers were noted from 10 to 35 with Reynolds (Re) numbers extended from 4550 to 20,367. For 0.075 mass% ZnO@TiO_2/DW binary composite nanofluid, an increase in local Nusselt (Nu) was recorded from 10 to 32 for the similar Reynolds (Re) numbers. For 0.05 mass% of ZnO@TiO_2/DW binary composite nanofluid, the local Nusselt (Nu) numbers are recorded from 10 to 30 with the Reynolds (Re) number varying from 5849 to 24,544. Lastly, for 0.025 mass% of ZnO@TiO_2/DW binary composite nanofluids the Nusselt (Nu) number increased from 10 to 25 with the same range of the Reynolds (Re) number. This declining conduct at lower concentrations and Reynolds is credited to the agglomeration properties of ZnO and TiO_2 in the base fluid at the lesser value of Reynolds (Re) number and lower metal oxide (MO) surface area at the low concentrations. With the high value of Reynolds, the agglomeration properties for ZnO and TiO_2 nanoparticles decrease which supports the dispersion and stability of nanoparticles in the base fluid due to its proper mixing.

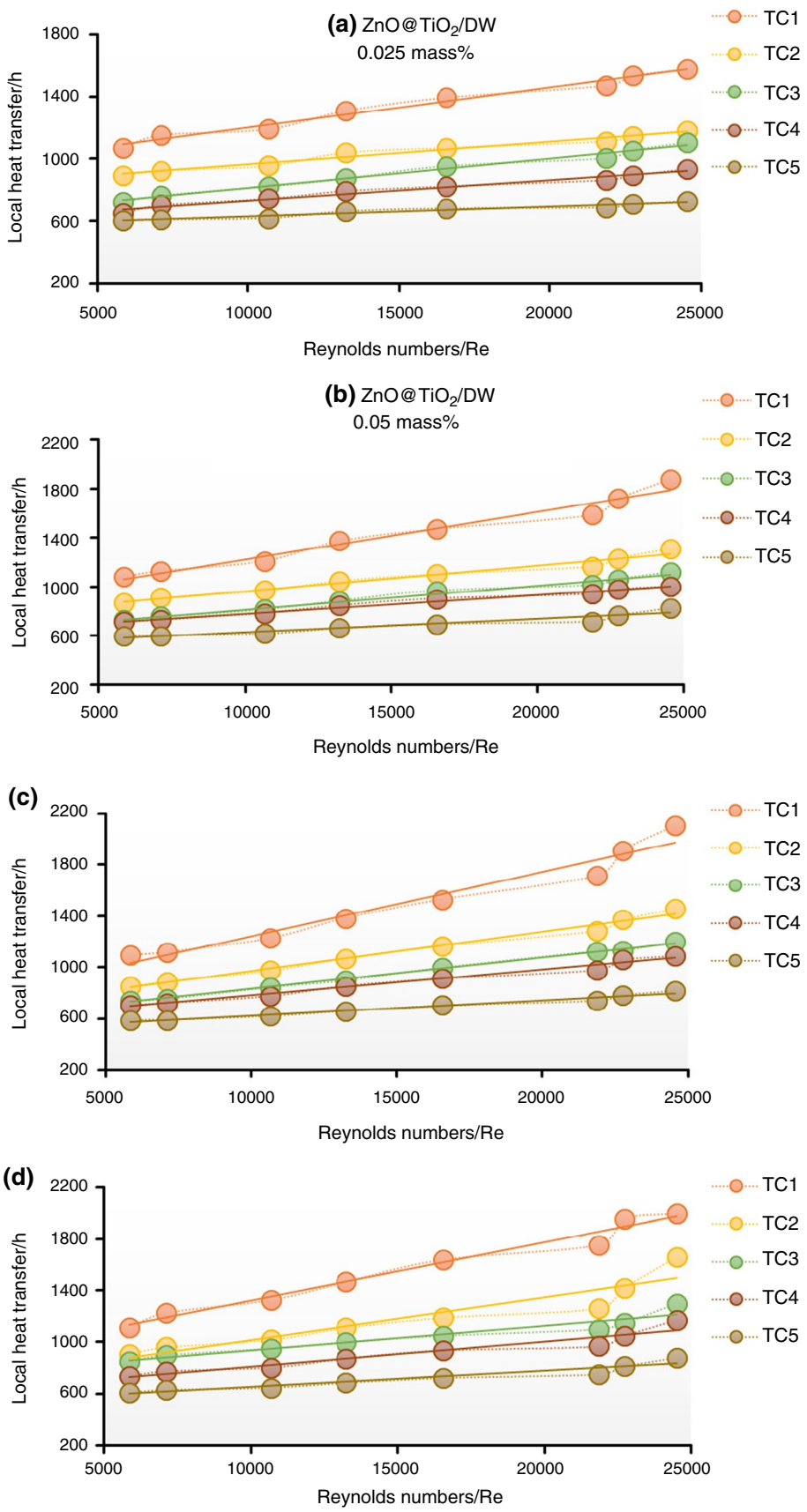

Fig. 14 Varriations in **a** local heat transfer calculations for 0.025 mass% and **b** local heat transfer calculations for 0.05 mass%, **c** local heat transfer calculations for 0.075 mass% and **d** local heat transfer calculations for 0.01 mass%, of ZnO@TiO_2/DW-based nanofluids

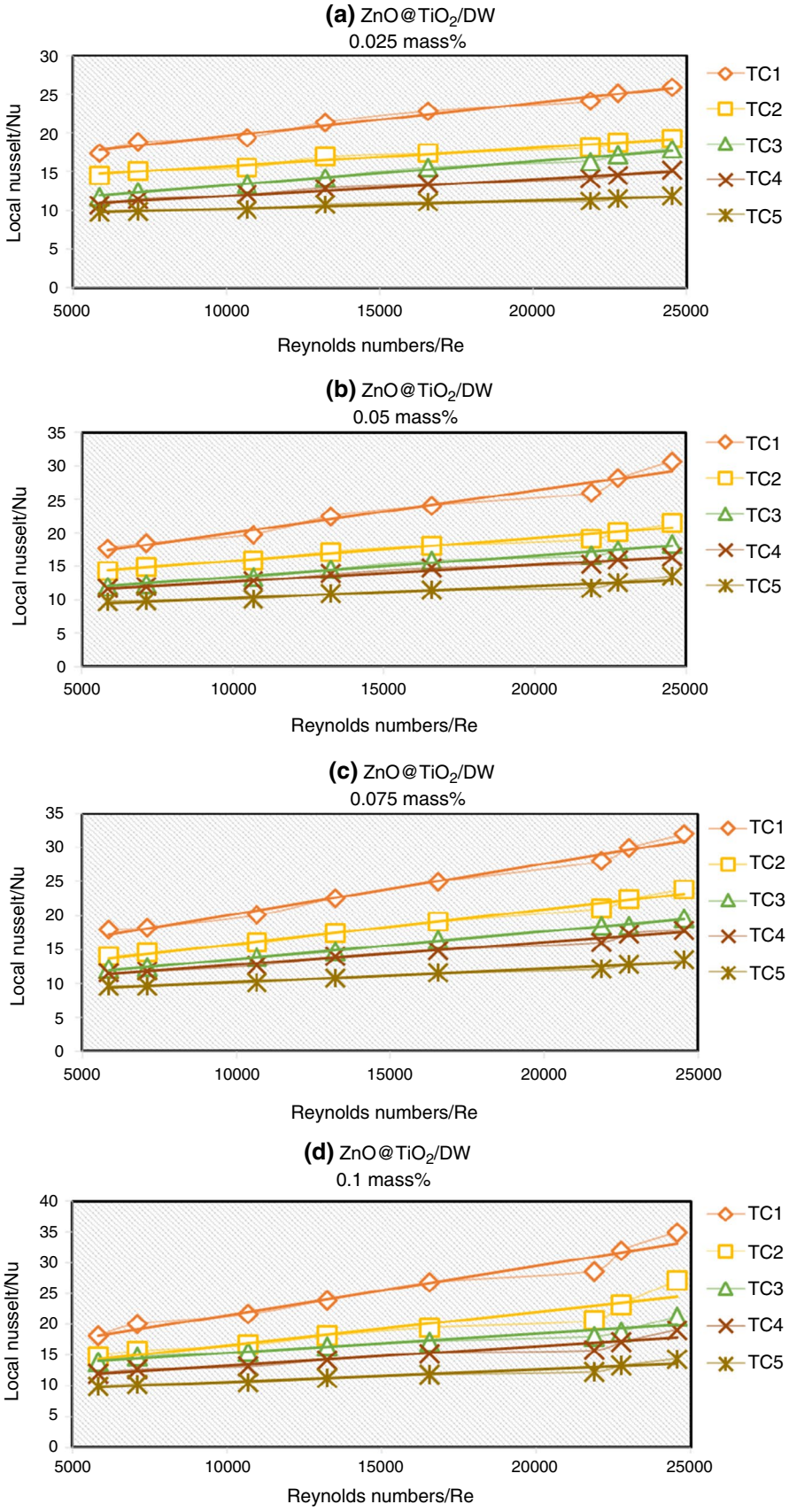

Fig. 15 Improvement in **a** local Nusselt numbers for 0.025 mass% and **b** local Nusselt numbers for 0.05 mass%, **c** local Nusselt numbers for 0.075 mass% and **d** local Nusselt numbers for 0.01 mass%, of ZnO@TiO_2/DW binary composite nanofluids

Conclusions

In the current research, the effective thermal conductivity of ZnO@TiO_2/DW binary composite nanofluid is examined for 0.1, 0.075, 0.05 and 0.025 mass% of ZnO and TiO_2 concentrations at a range of temperatures from 20 to 45 °C. The outcomes of this research exposed the equal mass ratio 50:50 of the both ZnO and TiO_2 nanoparticles and represent the finest combination rendering to the effective thermal conductivity. The equivalent ratio develops the control parameters and enhances the heat transfer performance also. From the examination of thermophysical properties and rendering to the Reynolds range from 5849 to 24,544, the 0.1 mass% concentration of ZnO@TiO_2/DW binary composite nanofluids is anticipated to describe the greater thermal performances of the binary composite nanofluids. Consequently, local and average convective heat transfer values for all mass% concentration of ZnO@TiO_2/DW binary composite nanofluid and the base fluid (DW) were experimentally assessed at different hydrodynamic and thermal circumstances by using a circular heat exchanger and constant heat flux. The highest improvement in average heat transfer of ZnO@TiO_2/DW binary composite nanofluids was recorded for the 0.1 mass% at the different studied conditions. The experimental outcomes described the addition of ZnO and TiO_2 nanoparticles with 50:50 in base fluid (DW) gives the best combination as a binary composite to improve the heat transfer properties, which is the finest mixture for cooling and so many other applications.

Acknowledgements The authors gratefully acknowledge the UMRG Grant RP045C-17AET, UM Research University Grant GPF050A-2018, Institute of Advanced Studies, Nanotechnology and Catalysis Research Center, Department of Mechanical Engineering and the University of Malaya for the support to conduct this research work.

Compliance with ethical standards

Conflict of interest The authors declare that they have no competing interests.

References

1. Sadri R, Mallah AR, Hosseini M, Ahmadi G, Kazi SN, Dabbagh A. CFD modeling of turbulent convection heat transfer of nanofluids containing green functionalized graphene nanoplatelets flowing in a horizontal tube: comparison with experimental data. J Mol Liq. 2018;269:152–9.
2. Amani M, Amani P, Kasaeian A, Mahian O, Wongwises S. Thermal conductivity measurement of spinel-type ferrite $MnFe_2O_4$ nanofluids in the presence of a uniform magnetic field. J Mol Liq. 2017;230:121–8.
3. Chaurasia P, Kumar A, Yadav A, Rai PK, Kumar V, Prasad L. Heat transfer augmentation in automobile radiator using Al_2O_3–water based nanofluid. SN Appl Sci. 2019;1(3):257.
4. Sedeh RN, Abdollahi A, Karimipour A. Experimental investigation toward obtaining nanoparticles' surficial interaction with basefluid components based on measuring thermal conductivity of nanofluids. Int Commun Heat Mass Transf. 2019;103:72–82.
5. Esmaeili E, Rounaghi SA, Gruner W, Eckert J. The preparation of surfactant-free highly dispersed ethylene glycol-based aluminum nitride–carbon nanofluids for heat transfer application. Adv Powder Technol. 2019;30:2032–41.
6. Poongavanam GK, Kumar B, Duraisamy S, Panchabikesan K, Ramalingam V. Heat transfer and pressure drop performance of solar glycol/activated carbon based nanofluids in shot peened double pipe heat exchanger. Renew Energy. 2019;140:580–91.
7. Esfe MH, Rostamian H, Sarlak MR. A novel study on rheological behavior of ZnO–MWCNT/10w40 nanofluid for automotive engines. J Mol Liq. 2018;254:406–13.
8. Goodarzi M, Toghraie D, Reiszadeh M, Afrand M. Experimental evaluation of dynamic viscosity of ZnO–MWCNTs/engine oil hybrid nanolubricant based on changes in temperature and concentration. J Therm Anal Calorim. 2019;136(2):513–25.
9. Soylu SK, Atmaca İ, Asiltürk M, Doğan A. Improving heat transfer performance of an automobile radiator using Cu and Ag doped TiO_2 based nanofluids. Appl Therm Eng. 2019;157:113743.
10. Motevasel M, Nazar ARS, Jamialahmadi M. Experimental study on turbulent convective heat transfer of water-based nanofluids containing alumina, copper oxides and silicon carbide nanoparticles. J Therm Anal Calorim. 2019;135(1):133–43.
11. Selvakumar RD, Dhinakaran S. Nanofluid flow and heat transfer around a circular cylinder: a study on effects of uncertainties in effective properties. J Mol Liq. 2016;223:572–88.
12. Sadri R, Ahmadi G, Togun H, Dahari M, Kazi SN, Sadeghinezhad E. An experimental study on thermal conductivity and viscosity of nanofluids containing carbon nanotubes. Nanoscale Res Lett. 2014;9(1):151.
13. Poongavanam GK, Ramalingam V. Characteristics investigation on thermophysical properties of synthesized activated carbon nanoparticles dispersed in solar glycol. Int J Therm Sci. 2019;136:15–32.
14. Wang D, Saleh NB, Sun W, Park CM, Shen C, Aich N. Next-generation multifunctional carbon–metal nanohybrids for energy and environmental applications. Environ Sci Technol. 2019;53:7265–87.
15. Schroeder V, Savagatrup S, He M, Lin S, Swager T. Carbon nanotube chemical sensors. Nano Lett. 2018;119(1):599–663.
16. Fan J, Wang L. Review of heat conduction in nanofluids. J Heat Transf. 2011;133(4):040801.
17. Yang Y, Zhang ZG, Grulke EA, Anderson WB, Wu G. Heat transfer properties of nanoparticle-in-fluid dispersions (nanofluids) in laminar flow. Int J Heat Mass Transf. 2005;48(6):1107–16.
18. Nanda J, Maranville C, Bollin SC, Sawall D, Ohtani H, Remillard JT. Thermal conductivity of single-wall carbon nanotube dispersions: role of interfacial effects. J Phys Chem C. 2008;112(3):654–8.
19. Choi S, Zhang Z, Yu W, Lockwood F, Grulke E. Anomalous thermal conductivity enhancement in nanotube suspensions. Appl Phys Lett. 2001;79(14):2252–4.
20. Liu M-S, Lin MC-C, Huang I-T, Wang C-C. Enhancement of thermal conductivity with carbon nanotube for nanofluids. Int Commun Heat Mass Transf. 2005;32(9):1202–10.
21. Garg P, Alvarado JL, Marsh C, Carlson TA, Kessler DA, Annamalai K. An experimental study on the effect of ultrasonication on viscosity and heat transfer performance of multi-wall carbon nanotube-based aqueous nanofluids. Int J Heat Mass Transf. 2009;52(21–22):5090–101.
22. Yu W, Xie H, Li Y, Chen L, Wang QJC, Physicochemical SA. Experimental investigation on the thermal transport properties of ethylene glycol based nanofluids containing low

volume concentration diamond nanoparticles. Powder Technol. 2011;380(1–3):1–5.
23. Baby TT, Ramaprabhu S. Investigation of thermal and electrical conductivity of graphene based nanofluids. J Appl Phys. 2010;108(12):124308.
24. Hu Z, Srinivasan MJM, Materials M. Preparation of high-surface-area activated carbons from coconut shell. Microporous Mesoporous Mater. 1999;27(1):11–8.
25. Kadirvelu K, Palanival M, Kalpana R, Rajeswari SJBT. Activated carbon from an agricultural by-product, for the treatment of dyeing industry wastewater. Biresour Technol. 2000;74(3):263–5.
26. Bhattacharyya KG, Sharma A. Adsorption of Pb(II) from aqueous solution by *Azadirachta indica* (Neem) leaf powder. J Hazard Mater. 2004;113(1–3):97–109.
27. Adinata D, Daud WMAW, Aroua MK. Preparation and characterization of activated carbon from palm shell by chemical activation with K_2CO_3. Biresour Technol. 2007;98(1):145–9.
28. Hameed B, Daud F. Adsorption studies of basic dye on activated carbon derived from agricultural waste: *Hevea brasiliensis* seed coat. Chem Eng J. 2008;139(1):48–55.
29. Bharadwaj D, Lundquist P, Alstrom SJAJES. Carbon nanomaterial from tea leaves as an anode in lithium secondary batteries. Asian J Exp Sci. 2008;22:89–93.
30. Musa SD, Zhonghua T, Ibrahim AO, Habib MJR, Reviews SE. China's energy status: a critical look at fossils and renewable options. Renew Sustain Energy Rev. 2018;81:2281–90.
31. Li D, Fang W, Zhang Y, Wang X, Guo M, Qin XJI. Stability and thermal conductivity enhancement of silver nanofluids with gemini surfactants. Ind Eng Chem Res. 2017;56(43):12369–75.
32. Mahrukh M, Kumar A, Gu S, Kamnis S, Gozali E. Modeling the effects of concentration of solid nanoparticles in liquid feedstock injection on high-velocity suspension flame spray process. Ind Eng Chem Res. 2016;55(9):2556–73.
33. Singh G, Lopes E, Hentges N, Becker D, Ratner A. Experimental investigation of the settling characteristics of carbon and metal oxide nanofuels. arXiv preprint http://arxiv.org/abs/1911.12238.
34. Kumar N, Sonawane SS, eds. Convective heat transfer of metal oxide-based nanofluids in a shell and tube heat exchanger. In: Conference proceedings of the second international conference on recent advances in bioenergy research. Berlin: Springer; 2018.
35. Branson BT, Beauchamp PS, Beam JC, Lukehart CM, Davidson JLJAN. Nanodiamond nanofluids for enhanced thermal conductivity. ACS Nano. 2013;7(4):3183–9.
36. Shima PD, Philip J. Role of thermal conductivity of dispersed nanoparticles on heat transfer properties of nanofluid. Ind Eng Chem Res. 2014;53(2):980–8.
37. Angayarkanni S, Philip J. Role of adsorbing moieties on thermal conductivity and associated properties of nanofluids. J Phys Chem C. 2013;117(17):9009–19.
38. Moosavi M, Goharshadi EK, Youssefi A. Fabrication, characterization, and measurement of some physicochemical properties of ZnO nanofluids. Int J Heat Fluid Flow. 2010;31(4):599–605.
39. Gao J, Zheng R, Ohtani H, Zhu D, Chen G. Experimental investigation of heat conduction mechanisms in nanofluids. Clue on clustering. Nano Lett. 2009;9(12):4128–32.
40. Singh V, Gupta M, Kumar A, eds. Investigating the morphology and thermophysical properties of Al_2O_3 and CuO nanofluids. IOP conference series: materials science and engineering. IOP Publishing; 2019.
41. Chaudhari S, Chakule R, Talmale P. Experimental study of heat transfer characteristics of Al_2O_3 and CuO nanofluids for machining application. Mater Today Proc. 2019;18:788–97.
42. Rahbar K, Riasi A, Sangjoeei HKB, Razmjoo N. Heat recovery of nano-fluid based concentrating photovoltaic thermal (CPV/T) collector with organic rankine cycle. Energy Convers Manag. 2019;179:373–96.
43. Asadi A, Asadi M, Rezaniakolaei A, Rosendahl LA, Afrand M, Wongwises S. Heat transfer efficiency of Al_2O_3–MWCNT/thermal oil hybrid nanofluid as a cooling fluid in thermal and energy management applications: an experimental and theoretical investigation. Int J Heat Mass Transf. 2018;117:474–86.
44. Parsian A, Akbari M. New experimental correlation for the thermal conductivity of ethylene glycol containing Al_2O_3–Cu hybrid nanoparticles. Therm Anal Calorim. 2018;131(2):1605–13.
45. Safi M, Ghozatloo A, Shariaty NM, Hamidi A. Preparation of MWNT/TiO_2 nanofluids and study of its thermal conductivity and stability; 2014.
46. Nine M, Batmunkh M, Kim J, Chung H, Jeong H. Investigation of Al_2O_3–MWCNTs hybrid dispersion in water and their thermal characterization. J Nanosci Nanotechnol. 2012;12:4553–9.
47. Tahat MS, Benim AC, eds. Experimental analysis on thermophysical properties of Al_2O_3/CuO hybrid nano fluid with its effects on flat plate solar collector. Defect and diffusion forum. Trans Tech Publ; 2017.
48. Suresh S, Venkitaraj K, Selvakumar P, Chandrasekar M. Synthesis of Al_2O_3–Cu/water hybrid nanofluids using two step method and its thermo physical properties. Colloids Surf A Physicochem Eng Asp. 2011;388(1–3):41–8.
49. Esfe MH, Arani AAA, Rezaie M, Yan W-M, Karimipour A. Experimental determination of thermal conductivity and dynamic viscosity of Ag–MgO/water hybrid nanofluid. Int Commun Heat Mass Transf. 2015;66:189–95.
50. Yarmand H, Gharehkhani S, Ahmadi G, Shirazi SFS, Baradaran S, Montazer E. Graphene nanoplatelets–silver hybrid nanofluids for enhanced heat transfer. Energy Convers Manag. 2015;100:419–28.
51. Paul G, Philip J, Raj B, Das PK, Manna I. Synthesis, characterization, and thermal property measurement of nano-Al95Zn05 dispersed nanofluid prepared by a two-step process. Int J Heat Mass Transf. 2011;54(15–16):3783–8.
52. Abdolbaqi MK, Sidik NAC, Aziz A, Mamat R, Azmi W, Yazid M. An experimental determination of thermal conductivity and viscosity of BioGlycol/water based TiO_2 nanofluids. Int Commun Heat Mass Transf. 2016;77:22–32.
53. Yu W, Xie H. A review on nanofluids: preparation, stability mechanisms, and applications. J Nanomater. 2012;2012:1.
54. Ghadimi A, Saidur R, Metselaar H. A review of nanofluid stability properties and characterization in stationary conditions. Int J Heat Mass Transf. 2011;54(17–18):4051–68.
55. Fernandez-Seara J, Uhía FJ, Sieres J, Campo AJATE. A general review of the Wilson plot method and its modifications to determine convection coefficients in heat exchange devices. Appl Therm Eng. 2007;27(17–18):2745–57.
56. Holman JP, Gajda WJ. Experimental methods for engineers. New York: McGraw-Hill; 2001.
57. Xu S, Fu L, Pham TSH, Yu A, Han F, Chen L. Preparation of ZnO flower/reduced graphene oxide composite with enhanced photocatalytic performance under sunlight. Ceram Int. 2015;41(3):4007–13.
58. Jwo C-S, Jeng L-Y, Chang H, Teng T-P. Experimental study on thermal conductivity of lubricant containing nanoparticles. Rev Adv Mater Sci. 2008;18:660–6.
59. Habibzadeh S, Kazemi-Beydokhti A, Khodadadi AA, Mortazavi Y, Omanovic S, Shariat-Niassar M. Stability and thermal conductivity of nanofluids of tin dioxide synthesized via microwave-induced combustion route. Chem Eng J. 2010;156(2):471–8.
60. Lee K, Hwang Y, Cheong S, Kwon L, Kim S, Lee JJCAP. Performance evaluation of nano-lubricants of fullerene nanoparticles in refrigeration mineral oil. Curr Appl Phys. 2009;9(2):e128–31.
61. Yarmand H, Gharehkhani S, Shirazi SFS, Goodarzi M, Amiri A, Sarsam WS, et al. Study of synthesis, stability and

thermo-physical properties of graphene nanoplatelet/platinum hybrid nanofluid. Int Commun Heat Mass Transf. 2016;77:15–21.
62. Ghosh M, Ghosh S, Pabi S. Effects of particle shape and fluid temperature on heat-transfer characteristics of nanofluids. J Mater Eng Perform. 2013;22(6):1525–9.
63. Harandi SS, Karimipour A, Afrand M, Akbari M, D'Orazio A. An experimental study on thermal conductivity of F-MWCNTs–Fe_3O_4/EG hybrid nanofluid: effects of temperature and concentration. Int Commun Heat Mass Transf. 2016;76:171–7.
64. Kumar MS, Vasu V, Gopal AV. Thermal conductivity and rheological studies for Cu–Zn hybrid nanofluids with various basefluids. J Taiwan Inst Chem Eng. 2016;66:321–7.
65. Ahammed N, Asirvatham LG, Wongwises S. Entropy generation analysis of graphene–alumina hybrid nanofluid in multiport minichannel heat exchanger coupled with thermoelectric cooler. Int J Heat Mass Transf. 2016;103:1084–97.
66. Esfe MH, Wongwises S, Naderi A, Asadi A, Safaei MR, Rostamian H. Thermal conductivity of Cu/TiO_2–water/EG hybrid nanofluid: experimental data and modeling using artificial neural network and correlation. Int Commun Heat Mass Transf. 2015;66:100–4.
67. Duangthongsuk W, Wongwises S. Effect of thermophysical properties models on the predicting of the convective heat transfer coefficient for low concentration nanofluid. Int Commun Heat Mass Transf. 2008;35(10):1320–6.
68. Gnielinski V. New equations for heat and mass transfer in the turbulent flow in pipes and channels. NASA STI/Recon Tech Rep A. 1975;75:8–16.
69. Petukhov B. Heat transfer and friction in turbulent pipe flow with variable physical properties. Adv Heat Transf. 1970;6:503–64.